Scientific Reports

https://doi.org/10.1038/s41598-026-58985-y

Article in Press

The primate hippocampus constructs a dynamic internal model of rhythmic events

Received: 5 September 2025

Accepted: 17 June 2026

Published online: 26 June 2026

Cite this article as: Salgado-Ménez M., Malagón A.M., Mercado K. *et al.* The primate hippocampus constructs a dynamic internal model of rhythmic events. *Sci Rep* (2026). https://doi.org/10.1038/s41598-026-58985-y

Mildred Salgado-Ménez, Ana M. Malagón, Karla Mercado & Victor de Lafuente

The Primate Hippocampus Constructs a Dynamic Internal Model of Rhythmic Events

Mildred Salgado-Ménez[1,†], Ana M. Malagón[1, 2,†], Karla Mercado[1], Victor de Lafuente[1,*].

[1]Institute of Neurobiology, National Autonomous University of Mexico.

Boulevard Juriquilla 3001, Querétaro, QRO., México, 76230.

[2]Biological Sciences Doctorate Program. National Autonomous University of Mexico.

Unidad de Posgrado, Ciudad Universitaria, CDMX, México, 04510.

[†]These authors contributed equally to this work.

*Correspondence: lafuente@unam.mx

Keywords: internal model, hippocampus, monkey, rhythm, time.

Abstract

The hippocampus contributes to the formation of internal representations that organize experience across space and time. Yet how it represents events that unfold continuously, especially when sensory input is absent and dynamics must be internally sustained, remains unclear. We recorded single-neuron and local field potential activity in the hippocampus of rhesus monkeys performing a metronome task in which a visual stimulus alternated rhythmically between two spatial locations and then had to be tracked internally without external cues. Hippocampal neurons exhibited tempo-scaled oscillatory firing patterns that correlated with stimulus location during a visible entrainment and an internal maintenance epoch. These dynamics compressed or stretched to match interval duration and were accompanied by broadband LFP power modulations that also scaled with tempo. In error trials oscillatory activity showed systematic phase shifts, and oscillation-related population components were attenuated, suggesting that hippocampal dynamics reflected the animals' internal estimates of stimulus position. Regression analyses revealed mixed selectivity, with firing rates influenced by spatial alternation, tempo context, elapsed time, and task epoch. These findings indicate that hippocampal populations generate dynamical activity that continuously track and predict the evolving spatiotemporal structure of ongoing events. Rather than representing time as an isolated variable, the primate hippocampus implements a predictive internal model linking temporal structure, spatial information, and contextual state to guide behavior in the absence of sensory input.

Significance statement

This study uncovers how primate hippocampal neurons represent dynamic events during both external perception and internal tracking. We observed that many hippocampal neurons display tempo-scaled oscillatory firing patterns that correlate with stimulus location both when visible and when tracked mentally. These oscillations showed systematic phase shifts during error trials, suggesting they reflect internal estimates of stimulus position. The results

show that the primate hippocampus supports internal models by continuously mapping the evolving spatiotemporal structure of both perceived and imagined events.

Introduction

The brain constructs internal models of the world to understand and anticipate environmental dynamics. These models integrate relationships between time, space, objects, and their potential causal connections[1-3]. By incorporating the spatial and temporal structure of events, internal models guide appropriate behavioral responses[4-7]. The hippocampus plays a central role in these processes, with its well-established ability to generate spatial maps that support navigation toward objects and locations[8-10]. In rodents, it has also been shown to represent temporal structure via time cells, which increase their activity at specific moments during a time interval, enabling the tracking of elapsed time[11-16]. This temporal coding allows the hippocampus to represent sequences of behaviorally relevant events. Thus, the hippocampus is thought to construct cognitive maps that integrate spatial and temporal information about the external world[17-21].

While rodent studies have established that the hippocampus represents temporal structure through time cells showing discrete activity peaks at specific moments during a delay interval[22-24], critical gaps remain in understanding how the primate hippocampus reflects continuously evolving temporal dynamics. First, classical time cell paradigms typically examine static intervals between discrete events, leaving unclear how hippocampal circuits represent rhythmic sequences that unfold continuously over time. Second, although recent studies have reported temporal correlates in the primate hippocampus[25-28], most employed tasks in which time was secondary to other behavioral demands such as working memory or spatial navigation, preventing direct assessment of temporal representation mechanisms. Third, the extent to which primate hippocampal neurons utilize oscillatory dynamics that scale with task tempo, rather than reflecting generic state dependent rhythms, remains unexplored. These limitations have been difficult to overcome because traditional experimental paradigms do not require continuous internal maintenance of temporally structured sequences in the absence of external cues, making it difficult to dissociate sensory driven activity from internally generated temporal representations.

We employed a metronome task in which primates observed and then internally maintained the spatial position of a visual stimulus that alternated between left and right at varying tempos[29-31]. Unlike traditional time cell paradigms that focus on isolated intervals, this task required continuous tracking of a dynamic spatiotemporal sequence, allowing direct examination of how temporal and spatial information are jointly represented when time is the primary behavioral variable. Prior work from our lab, based on population averages from a single monkey, revealed oscillatory activity in the hippocampus during this task[31]. Here, using extensive single unit recordings in two monkeys, we show that individual hippocampal

neurons exhibit tempo scaled oscillatory firing patterns that correlate with stimulus location both when the metronome is visible and when it is internally tracked. These dynamics differ from the discrete activity peaks expected from classical time cell models. By analyzing error trials, we further demonstrate that these oscillatory patterns reflect the monkeys' internal estimates of metronome position, providing evidence that hippocampal activity tracks subjective temporal structure rather than physical stimulus timing alone. Our results support the view that time in the hippocampus is not represented as an isolated variable, but is embedded within the evolving states of behaviorally relevant events, both external and internal[32-34].

Results

Monkeys track an internally sustained metronome with scalar timing behavior

Two rhesus monkeys performed a metronome task in which they fixated on and touched the center of a screen displaying a visual stimulus alternating between left and right positions (Fig. 1A). After observing three entrainment intervals, the visual stimulus disappeared, and the monkeys had to internally track the position of the non-visible stimulus during a maintenance epoch consisting of 1–6 intervals (randomly chosen). The trial ended when the hand fixation area disappeared (go-cue), prompting the monkeys to make a reach movement to indicate their estimated stimulus location.

Behavioral results show that the probability of correctly identifying the non-visible stimulus was high early in the maintenance period but decreased as a function of elapsed time (Fig. 1B). This pattern was well described by a model incorporating the scalar property of timing, where variability in time estimates increased with total elapsed time[35,36]. As time progressed during the maintenance epoch, the monkeys' internal metronome increasingly lagged or advanced relative to the true stimulus position, reducing the likelihood of correct responses (Fig. 1B, continuous line). This behavioral pattern was consistent across tempos (500, 750, and 1000 ms), demonstrating the monkeys' ability to adjust the tempo of an internal metronome on a trial-by-trial basis. Thus, the metronome task consisted of a dynamic stimulus that was first visible and subsequently maintained internally, allowing us to study hippocampal neuronal activity related to tracking both external and internal dynamic events.

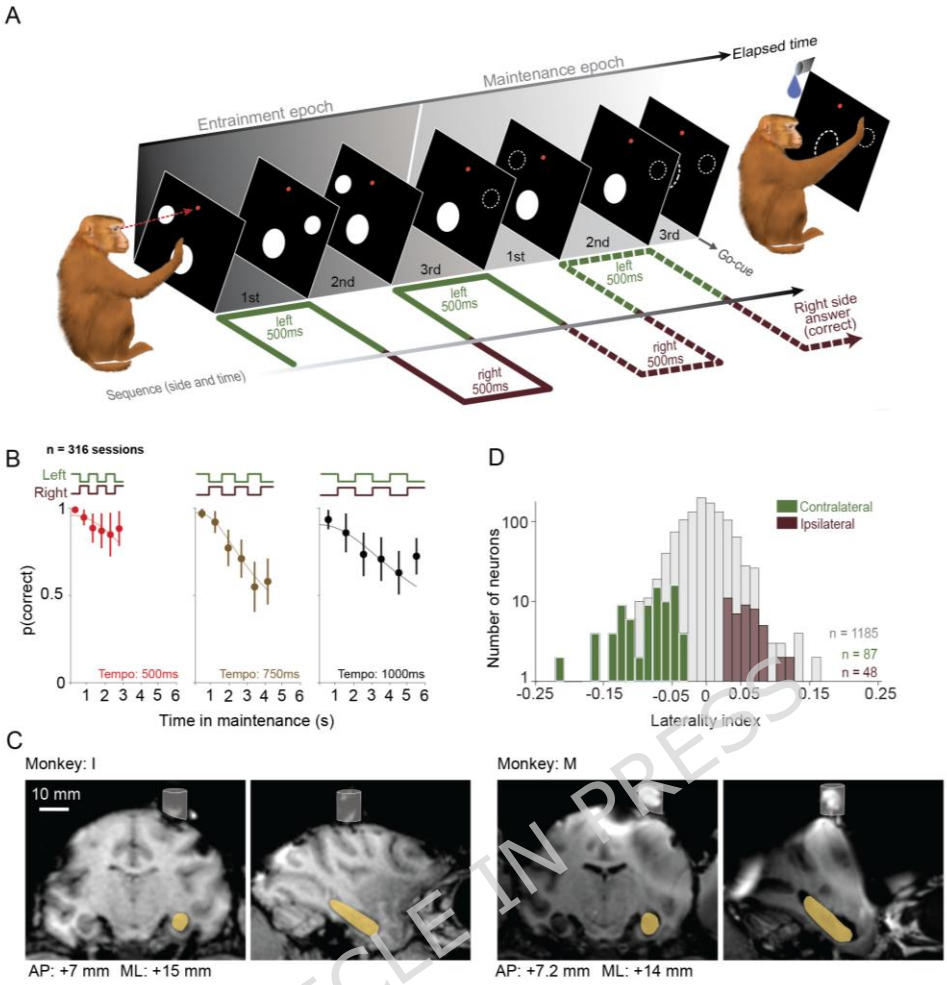

Figure 1. Metronome task design and behavioral performance.

(A) Monkeys observed a white circle alternating between left and right locations at one of three tempos (0.5, 0.75, 1s; randomly selected). After 3 entrainment intervals, the stimulus disappeared and monkeys internally tracked its position during 1-6 maintenance intervals (3 shown). Monkeys maintained central eye fixation and hand position until the go-cue.

(B) Behavioral performance measured as probability of correctly identifying metronome location p(correct) versus maintenance epoch time (mean ±IQR, 316 sessions). Probability of correct responses declined with time during the maintenance epoch. Performance was well captured by a model incorporating the scalar property of timing[29] (continuous colored line).

(C) Recording chambers were centered at stereotactic coordinates 9 mm anterior and 12 mm lateral relative to ear bar zero (EBZ), allowing vertical electrode access to the hippocampus (coronal and sagittal images from both monkeys).

(D) Distribution of laterality index (LI) values for all neurons (n=1185). Gray bars show non-significant LIs; colored bars indicate significant LIs (green: neurons with greater activation for contralateral stimuli, n=87; red: neurons preferring ipsilateral stimuli, n=48).

Hippocampal neurons show tempo-scaled oscillations during visible and non-visible metronome intervals

While the monkeys performed the metronome task, we recorded the extracellular spike potentials of 1408 hippocampal neurons (Fig. 1C; Methods). A large proportion of neurons (84%; 1185/1408) showed changes in firing rate during the task relative to the inter-trial period (*t*-test, $p<0.01$; FDR-corrected). Spatial selectivity was low, with a population mean laterality index of -0.038 $\pm$0.016 (95% CI; Fig. 1D), and 55% (648/1185) of neurons showing a negative laterality index, indicating a slight preference for visual stimuli presented in the left visual field (contralateral to the recorded hemisphere).

Many hippocampal neurons exhibited oscillatory firing dynamics during the metronome task. The examples in Fig. 2A and 2B illustrate two key features. First, firing rates oscillated in synchrony with the left–right alternation of the metronome, including during the maintenance epoch when the stimulus was no longer visible and had to be internally tracked. Second, both the overall firing rate profile and the oscillatory component scaled with metronome tempo, with cycles compressed at faster tempos and stretched at slower tempos. Because starting location and tempo were randomly selected on each trial, these tempo-scaled dynamics indicate flexible, trial-by-trial adjustment to the externally imposed rhythm that persisted during internal maintenance. In addition to rhythmic modulation, many neurons displayed slower monotonic trends across the trial, consistent with sensitivity to total elapsed time spanning entrainment and maintenance.

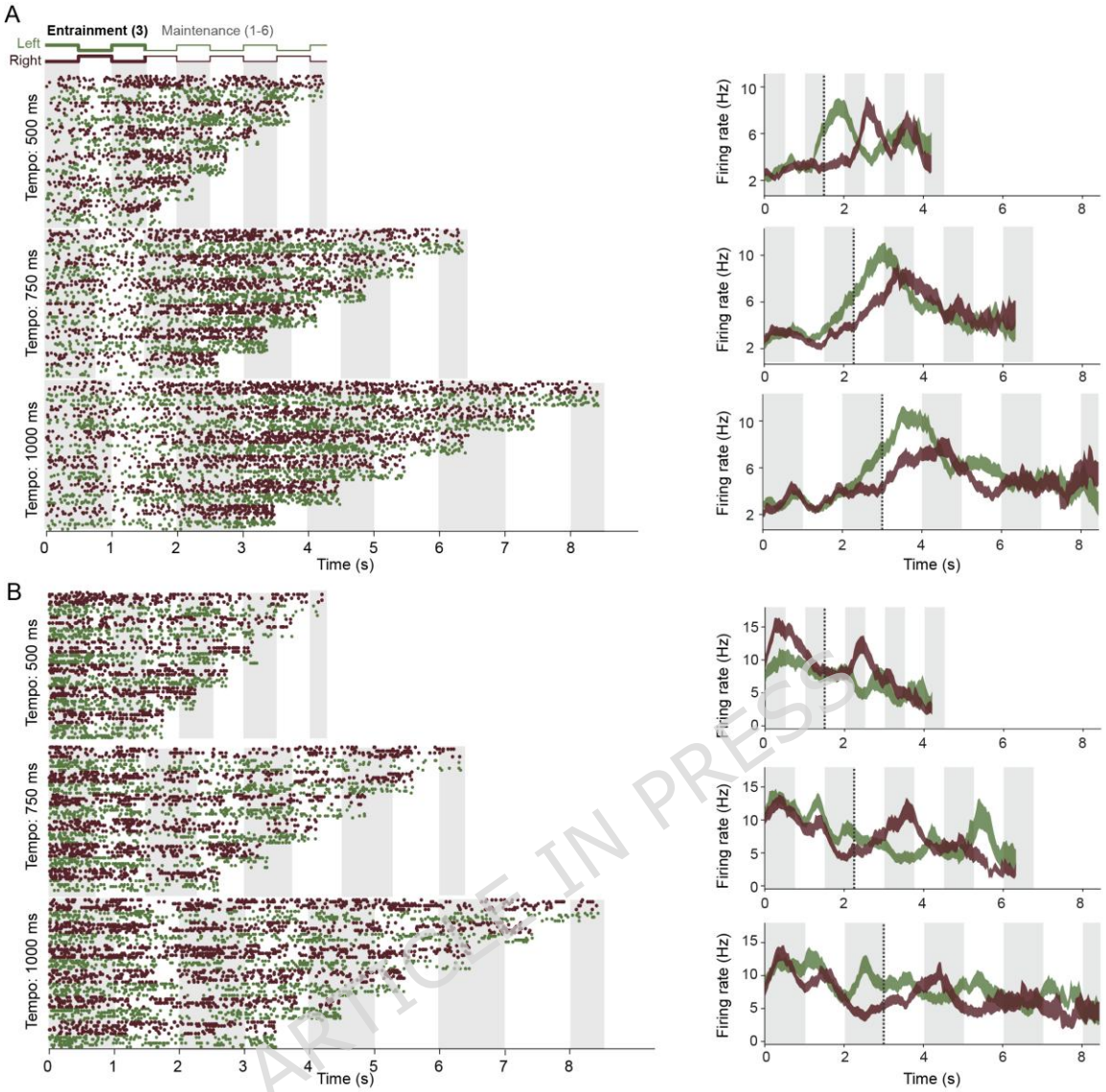

Figure 2. Raster plots and mean firing rates of example hippocampal neurons during the metronome task.

Each panel shows spike rasters aligned to metronome onset (left) and mean firing rates (right) plotted separately for the three tempos and the two starting locations (red, green).

(A) This neuron exhibited oscillatory firing significantly correlated with the left–right alternation of the metronome during the maintenance epoch when the stimulus was no longer visible demonstrating that activity tracked the internally maintained metronome position (cross-correlation between firing rate and stimulus position during maintenance r_{500}=0.45, r_{750}=0.34, r_{1000}=0.40; p<0.01).

(B) This neuron displayed oscillatory modulation and a gradual decrease in firing rate across the trial. The oscillatory components were significantly correlated with stimulus position (r_{500}=0.24, r_{750}=0.36, r_{1000}=0.42; p<0.01). In addition, firing rates showed negative slopes indicating progressive reduction of activity with increasing elapsed time (b_{500}=-1.78, b_{750}=-1.57, b_{1000}=-0.98 spk/s; p<0.01). These examples show that hippocampal neurons track rhythmic spatial alternation and global temporal progression, illustrating the mixed and dynamic nature of task-related modulation.

At the population level, hippocampal activity showed robust tempo-scaled oscillations that tracked the alternating left–right position of the metronome (Fig. 3A). The mean z-

scored firing rate across all task-responsive neurons (n = 1,185), aligned to metronome onset, revealed rhythmic modulations phase-locked to stimulus position that persisted throughout maintenance, indicating internally sustained temporal representations rather than purely stimulus-driven responses. A slower trial-wide modulation was superimposed on these oscillations. Cross-correlation between detrended firing rates and stimulus position during maintenance confirmed systematic alignment across tempos (r_{500}=0.28, r_{750}=0.21, r_{1000}=0.31; p<0.05; Sup. Fig. 2). Autocorrelation of the population mean further demonstrated tempo scaling, with the first negative peak shifting to longer lags for slower tempos (Fig. 3B, left). To verify that these population oscillations reflected genuine single-neuron dynamics rather than averaging artifacts, we estimated each neuron's oscillation period from its individual autocorrelation. The resulting period distributions were tightly centered on the true metronome tempo for each condition (Fig. 3B, right), demonstrating that individual hippocampal neurons exhibit tempo-scaled oscillatory firing on a trial-by-trial basis.

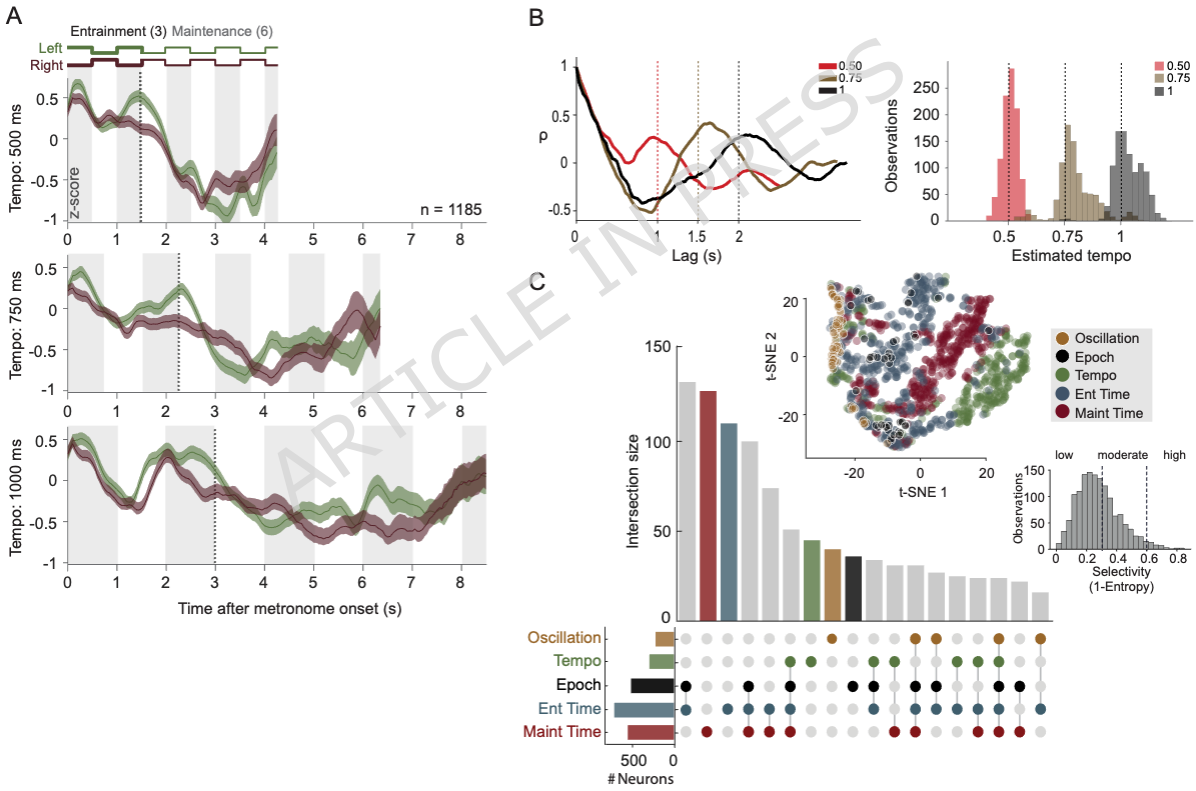

Figure 3. Tempo-scaled oscillatory dynamics and mixed selectivity in hippocampal populations.

(A) Mean z-scored firing rate across task-modulated hippocampal neurons (n = 1,185) aligned to metronome onset for the three tempos (500, 750, 1000 ms). Green and red traces correspond to left- and right-starting trials. Shaded regions indicate ± s.e.m. Alternating gray and white bands mark successive metronome intervals. The dashed vertical line indicates the transition from entrainment (3 visible intervals) to maintenance (internally tracked intervals). Population activity exhibits oscillations phase-locked to stimulus position that scale with tempo and persist during maintenance.

(B) Autocorrelation analyses of oscillatory dynamics. Left, autocorrelation of the population mean firing rate during maintenance for each tempo, showing tempo-dependent periodicity. Right, distribution of single-neuron

oscillation periods estimated from individual autocorrelograms. Dashed lines indicate the true metronome tempos. Period estimates cluster around the corresponding task tempo, demonstrating genuine tempo-scaled oscillations at the single-neuron level.

(C) GLM-based modulation analysis. Bottom horizontal bars show the number of neurons significantly modulated by each parameter family (oscillation, tempo, epoch, elapsed time during entrainment, elapsed time during maintenance). Vertical bars show the number of neurons significantly modulated by specific combinations of parameters. The largest intersections correspond to combinations of epoch and elapsed time, reflecting strong modulation by global task structure. Inset, t-SNE projection of neurons based on their ΔR^2 modulation profiles. Each point represents one neuron, colored by the parameter contributing the largest ΔR^2. The distribution of the entropy-based selectivity index (right inset) indicates predominantly mixed selectivity across task variables.

To quantitatively capture the dynamic activity patterns of individual hippocampal neurons we modeled single neuron firing rates using a generalized linear model (GLM) framework, in which firing rate was expressed as a linear combination of the following time-dependent metronome-related regressors: (1) tempo of the metronome, (2) spatial location, (3) trial epoch (entrainment, maintenance), (4) elapsed time in entrainment, and (5) elapsed time in maintenance. The influence of each regressor over the activity of hippocampal neurons was estimated by the ΔR^2 that was lost by dropping each regressor independently and its statistical significance was assessed by permutation analysis (Methods). The results are presented in an upset plot (Fig. 3C), showing the number of significant neurons for each regressor ("set size" horizontal bar plot), and the combination of significant regressors that was observed across neurons ("intersection size" vertical bar plot). Hippocampal neurons were significantly modulated by elapsed time, that is, they showed changes in firing rate, either increasing or decreasing, that were proportional to the absolute time within either the entrainment (n=689) or the maintenance epoch (n=533). The neurons also showed differences in firing rate across the entrainment and maintenance epochs (n=496; modeled as a step function in the GLM), that is, they distinguished whether the stimulus was visible or internally maintained. It is relevant to note that the first six intersections are combinations of epoch and elapsed time, which is consistent with recent findings showing that most of the variance of neurons recorded in behaving animals is explained by the overall temporal structure of the task[37-39].

Critically for the metronome task, hippocampal neurons were sensitive to the tempo of the metronome, not just by proportionally scaling its oscillation period (Fig. 3B), but also by systematic changes in the mean firing rate observed for each tempo (n=284; modeled as a scalar in the GLM). This suggests that tempo is represented not merely as a rescaling of time, but as a contextual variable that defines the operating regime of the internal dynamical model. Thus, hippocampal activity reflects a joint representation of phase within the sequence and global temporal context, consistent with a state-based internal model rather than an explicit clock. As previously shown by the autocorrelogram analysis, the GLM

demonstrate that neurons were sensitive to the spatial location of the metronome (n=212). It is important to note that, consistent with recent large-scale encoding studies[40], our GLM explains a modest fraction of single-neuron firing rate variance (~1.8%), yet it reveals that hippocampal neurons have a relationship with the spatial and temporal attributes of a visually guided and internally maintained metronome.

The GLM analysis revealed that many hippocampal neurons were correlated with multiple task variables simultaneously, rather than being exclusively driven by a single temporal or spatial attribute of the metronome. To quantify how concentrated the explanatory weight of the GLM regressors was for each neuron, we computed a selectivity index based on the normalized entropy of the regression coefficients (see Methods). Values close to 1 indicate that the model's explanatory power is dominated by a single regressor, whereas values close to 0 indicate that contributions are distributed across multiple regressors, consistent with mixed selectivity. The distribution of this index across the population (Fig. 3C, inset) showed that most neurons had low selectivity values, with a large fraction below 0.3 and the majority below 0.6, indicating that for most neurons the explanatory weight of the model was shared across several temporal and spatial attributes of the metronome task. To visualize how neurons were distributed in the space defined by the five GLM parameters, we performed a dimensionality reduction (t-SNE; Fig. 3C inset) using, for each neuron, the change in explained variance (ΔR^2) associated with each regressor. No clustering or classification procedure was applied, and neurons were colored according to the regressor with the largest ΔR^2. The apparent organization arises from the continuous similarity of modulation profiles across neurons, rather than from discrete functional categories. Together, the entropy-based selectivity index and the t-SNE visualization indicate that hippocampal neurons span a continuum of mixed selectivity across temporal and spatial features of the task, rather than segregating into distinct classes.

Task-related LFP power dynamics scale with metronome tempo

Given the oscillatory firing observed in single neurons, we next asked whether similar dynamics were present at the network level. We analyzed the local field potential using time–frequency analysis of trials sorted by metronome tempo (Fig. 4A; Sup. Fig. 3). To assess whether LFP power was modulated by the alternating position of the metronome, we subtracted the power observed in right-starting trials from that observed in left-starting trials. The results show a broadband modulation of LFP power (1 to 25 Hz), in which power oscillated in relation to the left–right alternation of the metronome (Fig. 4A; cross-correlation between mean power and stimulus position r_{500}=0.41, r_{750}=0.27, r_{1000}=0.36; p<0.01). Importantly, autocorrelation functions of the band-averaged LFP power (Fig. 4B) showed periodicity that stretched in proportion to metronome tempo, mirroring the tempo dependence observed at the single-neuron level. These results indicate that hippocampal

network activity exhibits task related, tempo scaled dynamics that reflect the alternating position of the metronome during visible and internally maintained epochs.

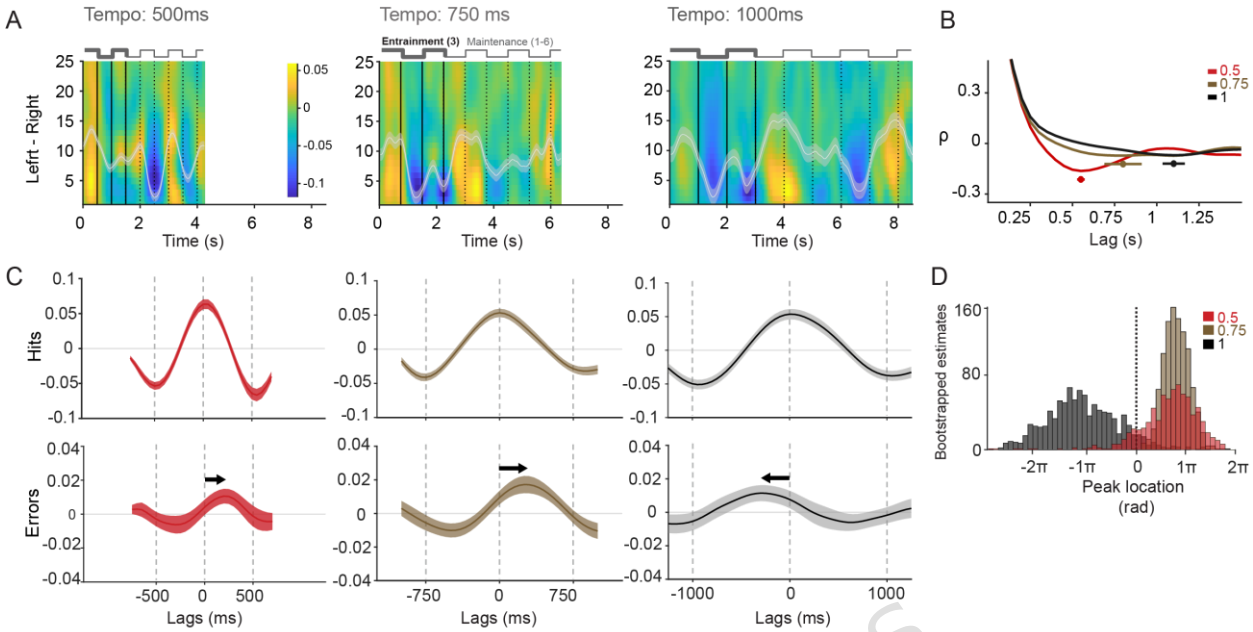

Figure 4. Task-related LFP dynamics and tempo-dependent phase shifts during error trials.

(A) Time–frequency representations of hippocampal LFP power for the three metronome tempos. Spectrograms show the difference in power between left-starting and right-starting trials. Broadband power (1–25 Hz; white trace, mean ± s.e.m.) oscillates in relation to the alternating metronome position. Cross-correlation between broadband LFP power and stimulus position during the maintenance epoch yielded peak values of r_{500}=0.67, r_{750}=0.53, r_{1000}=0.60 (p<0.01), indicating that LFP power modulations robustly track the internally maintained rhythm even in the absence of sensory input.

(B) Autocorrelation functions of band-averaged LFP power (1–25 Hz) for each tempo. The periodic structure scales with interval duration, with the first negative peak shifting to longer lags for slower tempos. Dots indicate the location of the most negative lag (mean ± s.e.m.).

(C) Cross-correlation between firing rate and stimulus position during the maintenance epoch. Upper row shows correct trials, revealing significant oscillatory coupling for all tempos. Lower row shows error trials. For fast and medium tempos, cross-correlation peaks shift toward negative lags, indicating that internal dynamics lag behind the true metronome position. For the slow tempo, peaks shift toward positive lags, indicating that internal dynamics lead the stimulus. Shaded areas denote s.e.m.

(D) Bootstrap distributions of phase shifts between correct and error trials for each tempo. Phase shifts were computed as the displacement of the cross-correlation peak in error trials relative to correct trials. Negative values indicate that the internal metronome lags the stimulus, whereas positive values indicate that it runs ahead. Median phase shifts differ significantly from zero (p<0.01), demonstrating systematic tempo-dependent deviations during incorrect performance.

The internal metronome is out of sync during error trials

We next examined whether hippocampal firing patterns during error trials reflected deviations in the internal tracking of the metronome. Previous behavioral studies have shown that during rapid metronomes subjects tend to fall behind the correct tempo, while during slow tempos they tend to get ahead[29]. We conducted cross-correlation analyses to

compare neuronal activity with the metronome's actual position during correct and error trials (Fig. 4C, upper row). As expected, neuronal oscillations in error trials were less consistent than in correct trials, i.e., the cross-correlation values between neuronal activity and stimulus position were significantly smaller on error trials. Moreover, the results show that, for fast metronomes error trial activity lagged behind correct trial activity, while for slow metronomes it led ahead of it (Fig. 4C, lower row). Bootstrap analysis confirmed these systematic phase shifts in error trials relative to correct trials (Fig. 4D; Methods). These findings provide further evidence that hippocampal activity reflects an internal, subjective representation of metronome position, supporting the role of the hippocampus in maintaining and updating a dynamic internal model of the metronome temporal structure.

Population correlates of rhythmic timing and elapsed time

Having established that hippocampal activity exhibits tempo-scaled oscillations, we next examined these dynamics at the population level. Principal component analysis of the recorded neurons revealed that the first three components combined slow trial-wide modulations with oscillatory activity aligned to the left–right alternation of the metronome during both entrainment and maintenance (Fig. 5A). Cross-correlations between each PC time series and stimulus position were all significant ($p<0.001$). PC1 crossed zero at lag zero, whereas PCs 2 and 3 were maximally correlated at lag zero in approximately opposite phase, indicating that rhythmic timing is distributed across multiple modes that capture complementary phases of the internally tracked metronome. These oscillatory patterns compressed for fast tempos and stretched for slow ones across both epochs (Fig. 5B), showing that low-dimensional population dynamics reflect rhythmic timing and elapsed time in register with the internally maintained metronome.

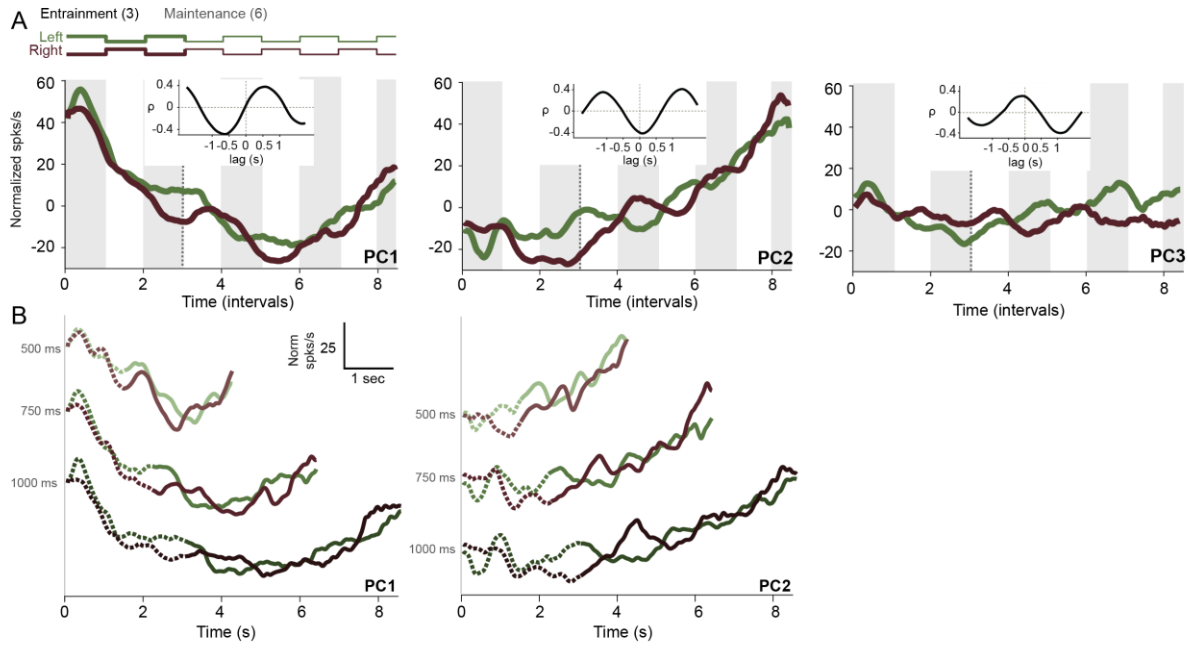

Figure 5. Population level principal components capture rhythmic timing and elapsed time.
(A) The first three principal components of population activity are plotted as a function of time expressed in interval units. Green and red traces correspond to left starting and right starting metronome trials, respectively. PC components show oscillatory modulations aligned with the left-right alternation of the metronome during both visible and internally maintained intervals. Insets show cross correlation functions between each detrended PC time series and stimulus position.
(B) The first two principal components are shown separately for each metronome tempo and starting location, plotted as a function of elapsed time in seconds. Dotted lines correspond to entrainment and solid lines to maintenance. Both the overall temporal profile and the oscillatory structure of the population activity scale systematically with metronome tempo across task epochs.

To dissociate how task variables contribute to these dynamics, we applied demixed principal component analysis (dPCA), which separates variance associated with specific parameters from condition-independent activity[37]. Condition-independent components captured 39% of the variance (Fig. 6A, D): dPC1 decreased monotonically across the trial, consistent with an elapsed-time correlate; dPC2 showed a U-shaped profile with elevated activity at trial onset and termination; and dPC5 peaked at the entrainment-to-maintenance transition, possibly reflecting the shift from sensory-driven to internally maintained tracking. Tempo-related components accounted for another 39% (Fig. 6B, D): dPC3 separated the 500 ms tempo from the 750 and 1000 ms tempos early in the trial, consistent with a potential perceptual similarity between the slower tempos, and also displayed rhythmic modulations at twice the left–right alternation frequency that were more pronounced during maintenance, possibly reflecting sensitivity to stimulus transitions rather than absolute spatial position. Spatial-location components explained 22% of the variance (Fig. 6C, D): dPC7 and dPC8 tracked stimulus position particularly during maintenance (dPC7 $r=0.51$; dPC8 $r=-0.61$; $p<0.01$), with an oscillatory pattern that appeared to omit the final entrainment interval, possibly reflecting predictive anticipation of the upcoming non-visible interval. Consistent with their functional relevance, these correlations were abolished in error trials (dPC7 $r=0.03$; dPC8 $r=-0.01$; $p>0.05$; Sup. Fig. 4). Together, these results indicate that hippocampal populations simultaneously reflect global trial structure, tempo, and spatial alternation, with these dynamical signals distributed across overlapping neural populations rather than segregated into distinct subpopulations.

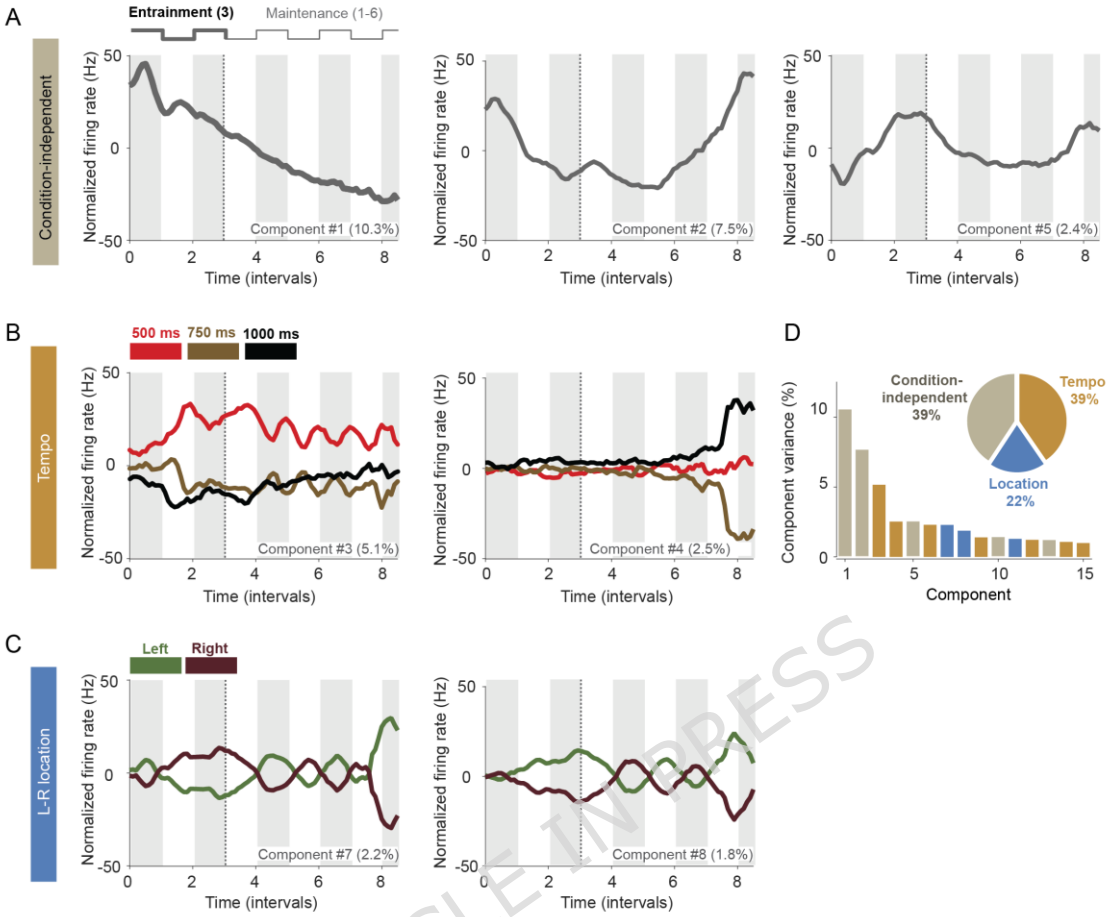

Figure 6. Demixed principal components reveal population correlates of elapsed time, tempo, and spatial alternation.

(A) Condition-independent components capture global trial structure. Components are plotted as normalized population activity as a function of time expressed in interval units, aligned to metronome onset. dPC1 shows a monotonic decrease across the trial, consistent with an elapsed time correlate. dPC2 exhibits a U-shaped profile with elevated activity at trial onset and termination. dPC5 peaks at the transition between entrainment and maintenance, possibly indicating the shift from sensory guided to internally maintained tracking.

(B) Tempo-related components. dPC3 separates the 500 ms tempo from the 750 and 1000 ms tempos early in the trial and displays rhythmic modulation aligned with stimulus transitions. Oscillations occur at twice the left–right alternation frequency and are more pronounced during maintenance. dPC4 captures additional tempo-dependent variance and shows divergence across tempos later in the trial.

(C) Spatial-location components. dPC7 and dPC8 exhibit oscillatory dynamics that track the left–right position of the metronome throughout the trial, particularly during maintenance (dPC7 r=0.51; dPC8 r=−0.61; $p<0.01$). Oscillatory structure diminishes during error trials (Sup. Fig. 4), indicating that spatially organized population dynamics are tightly linked to accurate internal tracking.

(D) Variance explained by the first 15 demixed components. Bar colors indicate the task parameter associated with each component. Pie chart summarizes the proportion of total variance attributed to condition-independent, tempo-related, and spatial-location components.

Discussion

Neurons in the primate hippocampus exhibited firing rate dynamics that tracked the rhythmic alternation of a visual metronome, and continued to do so when the stimulus was no longer visible and had to be maintained internally. These tempo-scaled oscillations persisted across entrainment and maintenance epochs, indicating that hippocampal activity reflects the evolution of a task-relevant internal representation rather than a purely stimulus-driven response. At both the single-neuron and population levels, hippocampal dynamics reflected spatial alternation, tempo context, elapsed time, and task phase, supporting the view that the hippocampus participates in constructing temporally structured internal models of ongoing events[21,41-43]. A key feature of the observed activity was its flexible temporal scaling[14,44,45]. Oscillatory firing patterns compressed or stretched to match the 500, 750, and 1000 ms tempos, demonstrating that hippocampal dynamics adapt on a trial-by-trial basis to an externally defined interval duration[46,47]. These oscillations were not limited to the period of sensory input but persisted during internal maintenance, when no external stimulus was present. This persistence indicates that hippocampal populations maintain a structured representation of the expected stimulus trajectory, consistent with theories proposing that the hippocampus supports predictive internal models that integrate space and time[16,48,49]. The functional relevance of these dynamics was revealed by error trials. When animals made incorrect judgments about stimulus position, hippocampal oscillations were systematically phase-shifted relative to correct trials, lagging for fast tempos and leading for slow tempos. These shifts mirror behavioral biases[29] and indicate that hippocampal activity reflects the animal's internal estimate rather than the physical stimulus location alone. At the population level, spatially structured components identified through demixed principal component analysis lost their correlation with stimulus position during error trials. The attenuation of oscillatory structure during incorrect performance suggests that accurate internal tracking depends on coordinated population dynamics rather than isolated neuronal responses[50,51]. Network-level analyses further support this interpretation. Local field potential power exhibited broadband 1-25 Hz modulations that tracked the left–right alternation of the metronome and scaled proportionally with tempo. These dynamics differ from canonical hippocampal rhythms associated with specific behavioral states, as their frequency was not fixed but instead matched the externally imposed tempo and persisted during internal maintenance. This pattern indicates that the oscillatory firing reported here reflects task-specific dynamical structure embedded within coordinated network activity[17,52,53]. Together with previous multi-area recordings[31] (Sup. Fig. 5), the present single-neuron and network-level analyses provide new insight into how hippocampal activity contributes to the representation of time and rhythm encoding within a distributed brain-wide circuit. We note that our conclusions rest on statistical relationships between hippocampal activity and task

variables; establishing a causal contribution of these dynamics will require future studies employing targeted perturbations.

GLM analyses revealed that hippocampal neurons rarely encoded a single task variable in isolation. Instead, firing rates were influenced simultaneously by spatial location, tempo, elapsed time within entrainment and maintenance, and the transition between these epochs. Quantification of selectivity showed that explanatory weight (ΔR^2) was typically distributed across multiple regressors, indicating mixed selectivity rather than discrete functional classes. Although task variables accounted for a modest proportion of single-neuron firing rate variance (~1.8%), this magnitude is consistent with large-scale population studies across cortical and subcortical regions in which behaviorally relevant variables explain limited but reliable fractions of neural variability[40]. The presence of distributed, overlapping representations suggests that hippocampal populations operate as dynamical systems whose trajectories reflect multiple aspects of task structure simultaneously. Principal components revealed rhythmic trajectories aligned with stimulus alternation as well as slower components consistent with elapsed time. Demixed principal components separated variance related to global trial structure, tempo context, and spatial alternation, demonstrating that these signals, although partially dissociable, are expressed within overlapping neural populations. Components associated with the transition between entrainment and maintenance indicate shifts in behavioral context, whereas tempo-related components suggest that interval duration might serve as a global parameter shaping dynamical regimes in the hippocampus[54-56]. Our results are consistent with the context continuity framework[57] which suggests that the hippocampus maintains context through neural patterns that evolve smoothly over time. Within this view, the tempo-scaled oscillatory activity observed here reflects continuous pattern formation rather than transitions between discrete attractor states. Rather than representing time as an isolated variable, hippocampal activity embeds temporal information within the evolving state of a spatiotemporal sequence. The degradation of oscillatory coherence during error trials further supports the idea that these trajectories reflect internally maintained estimates of ongoing events.

Our findings extend the concept of hippocampal cognitive maps beyond static spatial representations to encompass continuously evolving spatiotemporal sequences. During the metronome task, hippocampal populations tracked the alternation of spatial positions, the global tempo context, the passage of elapsed time, and the shift from sensory guided to internally guided tracking. These representations were expressed across single neurons, low dimensional population trajectories, and network level LFP dynamics, and were tightly linked to behavioral accuracy. Rather than representing time as an isolated variable, hippocampal activity embedded temporal information within the evolving state of the task, integrating interval structure, spatial alternation, and contextual transitions into a coherent

representation that persisted in the absence of sensory input. Together, these results support the view that the primate hippocampus contributes to predictive representations that couple temporal structure and spatial information to guide behavior when external cues are unavailable.[21,58,59].

Methods

Metronome task: Monkeys were seated in a primate chair in front of a touchscreen monitor (ELO Touch 1939L), which displayed the visual stimulus and recorded the position of the left hand. Each trial began when monkeys fixated on a central red dot (0.3° diameter) and touched a central hand fixation area (5° diameter). After a variable pre-stimulus delay (200–600 ms), a white circle (the metronome) appeared at 25° eccentricity and alternated between the left and right sides of the screen at one of three tempos (0.5, 0.75, or 1 s per interval). The stimulus was continuously visible during each interval (i.e., filled intervals). After three visible intervals (entrainment epoch), the metronome disappeared, and monkeys were required to internally track its position across 1 to 6 non-visible intervals (maintenance epoch). At the end of the maintenance epoch, the disappearance of the hand fixation area served as a go-cue, instructing monkeys to indicate the stimulus's estimated location (left or right) by reaching toward that side of the screen. The starting location, tempo, and number of maintenance intervals were pseudo-randomly selected on each trial. The metronome position remained static after the go-cue, ensuring the task was not a moving-target interception task. Monkeys were required to maintain eye fixation and hold their response hand on the fixation area until the go-cue.

Neuronal recordings: Recordings were performed from the right hippocampus of two rhesus monkeys (Macaca mulatta) across 161 sessions from monkey M (11 years old, 9 kg) and 198 sessions from monkey I (12 years old, 12 kg). Monkey I participated in previous hippocampal recordings[31], but all the data from the two monkeys in the present report are new and have not been published before. Experimental procedures were approved by the Ethics in Research Committee of the Institute of Neurobiology, National Autonomous University of Mexico (protocol No. 118), and conformed to principles outlined in the Guide for Care and Use of Laboratory Animals (NIH, USA). Hippocampal neurons were recorded using an acute vertical guide tube housing a single tungsten-platinum electrode (80 µm external diameter; 2-3 megaohms; Thomas Recording, Giessen, Germany). The guide tube was vertically lowered during each recording session to 1 cm dorsal to the hippocampus, with the electrode traversing the remaining distance. The recording chamber was implanted using a large-animal stereotactic frame, with placement verified by structural magnetic resonance imaging (Fig. 1C). During recordings, hippocampal entry was identified by the appearance of spiking activity after the electrode passed through the electrically neutral fourth ventricle dorsal to the hippocampus. Extracellular spike potentials were recorded

using the Cerebus acquisition system (Blackrock Microsystems, Salt Lake City, UT, USA) at a 30 kHz sampling frequency. Recordings with stable spike potentials from at least three trials per experimental condition were included in analyses (minimum ~100 trials, typically ~350 trials). These data have not been previously published.

Identification of task-modulated neurons: To identify neurons modulated by the metronome task, we compared firing rates during task performance to firing rates during the inter-trial interval. For each neuron, we performed a paired, trial-by-trial t-test comparing the mean firing rate during the inter-trial interval (3–7 s before trial onset) with the mean firing rate during the entire metronome task period. A single firing-rate value was computed per trial using variable-length windows that spanned the full inter-trial interval and the full task duration. This comparison was performed without subdividing trials by tempo or starting location. Neurons were classified as task-modulated if this comparison reached statistical significance ($p<0.01$) after false discovery rate correction.

Analyses of firing rates: Trial-by-trial firing rates were computed by convolving spike trains with a causal exponential kernel with a 0.2 s decay constant. Trials were categorized into six experimental conditions based on three metronome tempos (0.5, 0.75, and 1s) and two starting locations (left or right). Normalized mean firing rates were calculated for each neuron across each experimental condition, followed by computation of the population mean z-score (Fig. 3A). To compute the autocorrelation functions for each tempo condition, we first detrended the population mean firing rates by subtracting the overall mean from the mean responses obtained in left- and right-starting trials. For each tempo, the detrended mean firing rates from left- and right-starting trials were concatenated, and the autocorrelation function was calculated from the resulting time series (Fig. 3B, left). To assess oscillatory dynamics at the single-neuron level, we applied the same de-trending procedure to each neuron individually and computed its autocorrelation function. The oscillation tempo for each neuron (Fig. 3B right) was defined as the time lag corresponding to the most negative value of the autocorrelation function, reflecting the half-cycle separation between alternating stimulus positions. The laterality index (Fig. 1D) was computed as the difference divided by the sum of firing rates for left versus right stimulus presentations, pooling all entrainment and maintenance intervals. Because this measure ignores phase alignment between neuronal oscillations and stimulus position, it likely underestimates the number of neurons modulated by the metronome's left–right alternation.

Single-neuron GLM model of firing rate: Single-neuron firing rates were modeled using ordinary least squares regression on smoothed firing rates (identity link, Gaussian noise), following conventions used in recent large-scale encoding analyses[40]. Spike trains were convolved with a causal exponential kernel (τ = 200 ms) and sampled in 20 ms time bins to obtain a continuous firing rate estimate. The full model was:

$$FR(t) = \beta_0 + \beta_1 \sin(2\pi f t) + \beta_2 \cos(2\pi f t) + \beta_3 Tempo + \beta_4 Epoch + \beta_5 Ent_{lin}(t) + \beta_6 Ent_{exp}(t) + \beta_7 Maint_{lin}(t) + \beta_8 Maint_{exp}(t) + \varepsilon(t)$$

where FR(t) is the smoothed firing rate at time bin t, and ε(t) is the residual. We retain the term GLM to emphasize the decomposition of firing-rate modulation into distinct metronome-related variables, following conventions used in recent large-scale encoding analyses[40]. Time within each trial was expressed in interval units, defined as elapsed time divided by the metronome interval. This normalization aligned all metronome tempos onto a common temporal axis and ensured that temporal scaling was captured by shared time-dependent regressors.

Regressors were organized into five parameter families. (1) Oscillatory modulation was modeled using paired sine and cosine regressors (β_1, β_2) evaluated at the task-specific frequency f, defined as the reciprocal of twice the metronome interval such that one full sinusoidal cycle corresponds to one left–right alternation. A phase offset was applied to right-starting trials to track alternating spatial location. This parameterization allows recovery of oscillation amplitude ($\sqrt{(\beta_1^2 + \beta_2^2)}$) and phase ($\arctan(\beta_2/\beta_1)$). (2) Metronome tempo ($\beta_3$) was modeled as a scalar regressor encoding the interval duration. (3) Task epoch (β_4) was modeled as a step function distinguishing entrainment from maintenance. (4) Elapsed time during entrainment was modeled using linear (β_5) and exponential (β_6; τ = 1.5 intervals) ramps active only during entrainment. (5) Elapsed time during maintenance was modeled using the corresponding linear (β_7) and exponential (β_8) ramps active only during maintenance. Because time was expressed in interval units, the temporal basis was normalized across tempi, so that differences in the rate of firing-rate change across tempos reflect genuine tempo-dependent modulation rather than differences in absolute elapsed time. Models were fit by ordinary least squares to the concatenated firing-rate time series across trials. The contribution of each parameter family was quantified as the change in explained variance (ΔR^2) obtained by removing that family from the full model and refitting. This measure reflects the unique variance attributable to each task variable after accounting for all others. Because firing rates exhibit temporal autocorrelation within trials, standard parametric tests of ΔR^2 significance can be biased toward false positives. We therefore assessed statistical significance using permutation procedures matched to the structure of each parameter. For oscillation, we shuffled the starting-side labels (left vs. right) across trials within each tempo stratum; for tempo, we shuffled the tempo labels across trials within each starting side. For task epoch and elapsed time within epoch, the firing-rate time series were circularly shifted within trials to preserve autocorrelation while disrupting alignment with regressors. 1000 permutations were used to estimate the null distributions. Neurons were classified as significant at $p<0.05$ after false discovery rate correction across the population.

As a complementary check, we evaluated whether model complexity could account for the observed effects by computing the change in Bayesian Information Criterion (ΔBIC = BIC_reduced − BIC_full) for each parameter family and neuron. BIC penalizes model complexity through an additive term proportional to the number of parameters and the logarithm of the sample size. BIC favored inclusion of these parameter families in a substantially larger proportion of neurons (ΔBIC>6) than the permutation tests across all five parameter families, confirming that the permutation-based criterion is more conservative than the standard complexity-penalized metric and that overfitting does not account for the effects we report. The encoding model explained a modest fraction of firing-rate variance at the level of individual neurons (mean 1.8% ± 2.8% s.d.). This magnitude is consistent with previous large-scale neural encoding studies[40] and reflects the high intrinsic variability of hippocampal firing, the sparse and mixed selectivity of individual neurons, and the use of fine temporal resolution. Even small fractions of explained variance can reliably identify task-related modulation across large neuronal populations.

Neuron selectivity for the metronome parameters: To quantify whether neurons were preferentially modulated by a single task variable or exhibited mixed selectivity, we computed a normalized entropy-based selectivity index derived from the explained variance profile across the five parameter families. For each neuron, contributions were expressed as proportions of total explained variance. Shannon entropy was calculated across these proportions and normalized by the maximum entropy for five categories. Selectivity was defined as 1-normalized entropy, yielding values between zero and one. Values near 0 indicate distributed modulation across multiple metronome variables, whereas values near 1 indicate dominance by a single variable. To visualize the distribution of modulation profiles across the population, we applied t-distributed stochastic neighbor embedding (t-SNE) to the five-dimensional vectors of explained variance after z-score normalization across neurons (perplexity=30). No clustering procedure was imposed. Neurons were colored according to the parameter family contributing the largest fraction of explained variance. Apparent grouping reflects graded similarity of modulation profiles rather than discrete functional categories.

Local field potential analysis: Local field potentials were recorded simultaneously with single-unit activity and aligned to metronome onset. Time–frequency representations were computed for each trial using a sliding window Fourier transform (spectrogram function in Matlab). Trials were grouped by metronome tempo and starting position. For each tempo, LFP power was averaged separately for left-starting and right-starting trials, and a difference spectrogram was obtained by subtracting right-starting from left-starting power. To summarize broadband fluctuations, LFP power was averaged across frequencies from 1 to 25 Hz, resulting a single LFP power signal for each tempo. To assess the temporal structure

of the LFP power, we computed the autocorrelation function, and the characteristic timescale (tempo) was estimated from the location (lag) of the negative peak in the autocorrelation function.

Phase shift analysis in error trials: To quantify phase differences between correct and error trials, we computed cross-correlation functions between neuronal firing rates and stimulus position during the maintenance epoch. For each neuron and tempo condition, cross-correlation functions were computed separately for correct and error trials. To facilitate visualization and comparison across tempos, the phase of the cross-correlation peak for correct trials was aligned to zero. Phase shifts in error trials were then defined as the displacement of the peak of the error-trial cross-correlation function relative to this zero-aligned reference. Statistical reliability of the phase shifts was assessed using a bootstrap procedure in which error trials were resampled with replacement and the location of the cross-correlation peak was recomputed for each resample. This procedure yielded a distribution of phase shifts for each tempo, and the median phase shift of each distribution was tested against zero and found to be significantly different from zero at the $p<0.01$ level, indicating systematic phase deviations in error trials relative to correct trials.

Principal component analysis (PCA): We conducted PCA on neuronal mean firing rates to identify latent dynamics in hippocampal population activity. PCA was performed using Matlab's *pca()* function on a matrix with N rows (neurons) and M columns (time points). Firing rates were sampled either at 20 ms intervals or 10 times per metronome interval. This allowed plotting PC components against time in either seconds or interval units. Data from the six experimental conditions (3 tempos x 2 starting locations) were concatenated along the time dimension (M). The first PC's temporal dynamics were plotted separately for each experimental condition. We also employed demixed-PCA (dPCA), which isolates activity dynamics associated with specific experimental parameters. For the metronome task, these parameters included tempo, spatial location, and condition-independent components capturing dynamics related to trial-wide patterns (Fig. 6). For dPCA analysis, firing rates were sampled 10 times per metronome interval, expressing time in interval units to standardize length across metronome tempos.

References

1. Friston, K. The free-energy principle: A unified brain theory? *Nat Rev Neurosci* **11**, 127–138 (2010).
2. O'Keefe, J. & Nadel, L. *The Hippocampus as a Cognitive Map*. (Clarendon Press, 1978).
3. Sun, W. *et al.* Learning produces an orthogonalized state machine in the hippocampus. *Nature* **640**, 165–175 (2025).
4. Behrens, T. E. *et al.* What is a cognitive map? Organizing knowledge for flexible behavior. *Nat Rev Neurosci* **19**, 655–665 (2018).

5. Clark, A. Whatever next? Predictive brains, situated agents, and the future of cognitive science. *Behavioral and Brain Sciences* **36**, 181–204 (2013).

6. Kaplan, R. & Friston, K. J. Planning and navigation as active inference. *Biol Cybern* **112**, 323–343 (2018).

7. Leon, M. I. & Shadlen, M. N. *Representation of Time by Neurons in the Posterior Parietal Cortex of the Macaque. Neuron* vol. 38(2), 317-27 (2003).

8. Ekstrom AD, Ranganath C. Space, time, and episodic memory: The hippocampus is all over the cognitive map. Hippocampus. 2018 Sep;28(9):680-687. doi: 10.1002/hipo.22750. Epub 2017 Jun 30. PMID: 28609014.

9. Hafting, T., Fyhn, M., Molden, S., Moser, M. B. & Moser, E. I. Microstructure of a spatial map in the entorhinal cortex. *Nature* **436**, 801–806 (2005).

10. O'Keefe, J. A computational theory of the hippocampal cognitive map. *Prog Brain Res* **83**, 301–312 (1990).

11. Buzsaki, G. & Tingley, D. Space and Time: The Hippocampus as a Sequence Generator. *Trends Cogn Sci* **22**, 853–869 (2018).

12. Mankin, E. A. *et al.* Neuronal code for extended time in the hippocampus. *PNAS* **109**, 19462–19467 (2012).

13. McNamee, D. C., Stachenfeld, K. L., Botvinick, M. M. & Gershman, S. J. Flexible modulation of sequence generation in the entorhinal–hippocampal system. *Nat Neurosci* **24**, 851–862 (2021).

14. Pastalkova, E., Itskov, V., Amarasingham, A. & Buzsaki, G. Internally generated cell assembly sequences in the rat hippocampus. *Science* **321**, 1322–1327 (2008).

15. Pfeiffer, B. E. & Foster, D. J. Hippocampal place-cell sequences depict future paths to remembered goals. *Nature* **497**, 74–79 (2013).

16. Reddy, L. *et al.* Human Hippocampal Neurons Track Moments in a Sequence of Events. *Journal of Neuroscience* **41**, 6714–6725 (2021).

17. Aronov, D., Nevers, R. & Tank, D. W. Mapping of a non-spatial dimension by the hippocampal-entorhinal circuit. *Nature* **543**, 719–722 (2017).

18. Epstein, R. A., Patai, E. Z., Julian, J. B. & Spiers, H. J. The cognitive map in humans: spatial navigation and beyond. *Nat Neurosci* **20**, 1504–1513 (2017).

19. Hampton, R. R., Hampstead, B. M. & Murray, E. A. Selective hippocampal damage in rhesus monkeys impairs spatial memory in an open-field test. *Hippocampus* **14**, 808–818 (2004).

20. Schiller, D. *et al.* Memory and space: Towards an understanding of the cognitive map. *Journal of Neuroscience* **35**, 13904–13911 (2015).

21. Stachenfeld, K. L., Botvinick, M. M. & Gershman, S. J. The hippocampus as a predictive map. *Nat Neurosci* **20**, 1643–1653 (2017).

22. Eichenbaum, H. On the Integration of Space, Time, and Memory. *Neuron* **95**, 1007–1018 (2017).
23. Howard, M. W. & Eichenbaum, H. Time and space in the hippocampus. *Brain Res* **1621**, 345–354 (2015).
24. Kraus, B. J. *et al.* During Running in Place, Grid Cells Integrate Elapsed Time and Distance Run. *Neuron* **88**, 578–589 (2015).
25. Bright, I. M. *et al.* A temporal record of the past with a spectrum of time constants in the monkey entorhinal cortex. *Proc Natl Acad Sci U S A* **117**, 20274–20283 (2020).
26. Naya, Y. & Suzuki, W. A. Integrating what and when across the primate medial temporal lobe. *Science (1979)* **333**, 773–776 (2011).
27. Sakon, J. J. & Suzuki, W. A. A neural signature of pattern separation in the monkey hippocampus. *Proc Natl Acad Sci U S A* **116**, 9634–9643 (2019).
28. Umbach, G. *et al.* Time cells in the human hippocampus and entorhinal cortex support episodic memory. *Proc Natl Acad Sci U S A* **117**, 28463–28474 (2020).
29. Garcia-Garibay, O., Cadena-Valencia, J., Merchant, H. & de Lafuente, V. Monkeys share the human ability to internally maintain a temporal rhythm. *Front Psychol* **7**, 1–12 (2016).
30. Cadena-Valencia, J., Garcia-Garibay, O., Merchant, H., Jazayeri, M. & DeLaFuente, V. Entrainment and maintenance of an internal metronome in supplementary motor area. *Elife* (2018).
31. de Lafuente, V. *et al.* Keeping time and rhythm by internal simulation of sensory stimuli and behavioral actions. *Sci Adv* **10**, (2024).
32. Davachi, L. & DuBrow, S. How the hippocampus preserves order: The role of prediction and context. *Trends Cogn Sci* **19**, (2015).
33. Ranganath, C. & Hsieh, L. T. The hippocampus: a special place for time. *Ann N Y Acad Sci* **1369**, 93–110 (2016).
34. Robbe, D. Lost in time: rethinking duration estimation outside the brain. *Neurosci Biobehav Rev* (2023) doi:10.31234/OSF.IO/3BCFY.
35. Gibbon, J. Scalar expectancy theory and Weber's law in animal timing. *Psychol Rev* **84**, 279–325 (1977).
36. Merchant, H., Harrington, D. L. & Meck, W. H. Neural Basis of the Perception and Estimation of Time. *Annu Rev Neurosci* **36**, 313–336 (2013).
37. Kobak, D. *et al.* Demixed principal component analysis of neural population data. elife. **5**, e10989 (2016).
38. Kaufman, M. T., Seely, J. S., Sussillo, D., Ryu, S. I., Shenoy, K. V., & Churchland, M. M. (2016). The Largest Response Component in the Motor Cortex Reflects Movement Timing but Not Movement Type. *eNeuro*, *3*(4), ENEURO.0085-16.2016.

39. Gallego, J. A., Perich, M. G., Naufel, S. N., Ethier, C., Solla, S. A., & Miller, L. E. (2018). Cortical population activity within a preserved neural manifold underlies multiple motor behaviors. Nature communications, 9(1), 4233. https://doi.org/10.1038/s41467-018-06560-z

40. International Brain Laboratory, Angelaki, D., Benson, B., Benson, J., Birman, D., Bonacchi, N., Bougrova, K., ... & Witten, I. B. A brain-wide map of neural activity during complex behaviour. *Nature* 645(8079), 177-191 (2025).

41. Buckner, R. L. The role of the hippocampus in prediction and imagination. *Annu Rev Psychol* **61**, 27–48 (2010).

42. Hasselmo, M. A model of episodic memory: mental time travel along encoded trajectories using grid cells. *Neurobiology of learning* (2009).

43. Whittington, J., Muller, T., Mark, S., Chen, G. & Barry, C. The Tolman-Eichenbaum machine: unifying space and relational memory through generalization in the hippocampal formation. *Cell* **183**, 1249–1263 (2020).

44. Rolando, F., Kononowicz, T. W., Duhamel, J. R., Doyère, V. & Wirth, S. Distinct neural adaptations to time demand in the striatum and the hippocampus. *Current Biology* **34**, 156-170.e7 (2024).

45. Shimbo, A., Izawa, E. I. & Fujisawa, S. Scalable representation of time in the hippocampus. *Sci Adv* **7**, (2021).

46. Wang, J., Narain, D., Hosseini, E. A. & Jazayeri, M. Flexible timing by temporal scaling of cortical responses. *Nat Neurosci* **21**, 102–112 (2018).

47. Mello, G. B. M., Soares, S. & Paton, J. J. A scalable population code for time in the striatum. *Curr. Biol.* **25**, 1113–1122 (2015).

48. Neupane, S., Fiete, I. & Jazayeri, M. Mental navigation in the primate entorhinal cortex. *Nature* **630**, 704–711 (2024).

49. Zutshi, I. *et al.* Hippocampal neuronal activity is aligned with action plans. *Nature* **639**, 153–161 (2025).

50. Elston, T. W. & Wallis, J. D. Context-dependent decision-making in the primate hippocampalprefrontal circuit. *Nat Neurosci* **28**, 374–382 (2025).

51. Omer, D. B., Las, L. & Ulanovsky, N. Contextual and pure time coding for self and other in the hippocampus. *Nat Neurosci* **26**, 285–294 (2023).

52. MacDonald, C. J., Lepage, K. Q., Eden, U. T. & Eichenbaum, H. Hippocampal 'time cells' bridge the gap in memory for discontiguous events. *Neuron* **71**, 737–749 (2011).

53. Sun, C., Yang, W., Martin, J. & Tonegawa, S. Hippocampal neurons represent events as transferable units of experience. *Nature Neuroscience 2020 23:5* **23**, 651–663 (2020).

54. Cruzado, N. A., Tiganj, Z., Brincat, S. L., Miller, E. K. & Howard, M. W. Conjunctive representation of what and when in monkey hippocampus and lateral prefrontal cortex during an associative memory task. *Hippocampus* **30**, 1332–1346 (2020).

55. Villette, V., Malvache, A., Tressard, T., Dupuy, N. & Cossart, R. Internally recurring hippocampal sequences as a population template of spatiotemporal information. *Neuron* **88**, 357–366 (2015).
56. Paton, J. J. & Buonomano, D. V. The Neural Basis of Timing: Distributed Mechanisms for Diverse Functions. *Neuron* **98**, 687–705 (2018).
57. Maurer, A. P., & Nadel, L. The continuity of context: a role for the hippocampus. *Trends in cognitive sciences*, 25(3), 187-199 (2021).
58. Chen, Y., Zhang, H., Cameron, M. & Sejnowski, T. Predictive sequence learning in the hippocampal formation. *Neuron* **112**, 2645–2658 (2024).
59. Rolls, E. T. & Mills, P. The generation of time in the hippocampal memory system. *Cell Rep* **28**, 1649–1658 (2019).

Data availability

Data is available from the corresponding author upon reasonable request.

Code availability

The analyses used standard functions and toolboxes included in Matlab (Mathworks). No new algorithms or specialized code was developed.

Acknowledgements

We thank Juan Ortiz and Pamela García for obtaining the MRI images; and Anaid Antaramian for support with the primate facility administration.

Funding

This work was supported by grants from UNAM-PAPIIT (IN207325) and from the Mexican Secretariat of Science, Humanities, Technology and Innovation (SECIHTI; CBF-2025-I-18). M. S-M. is a doctoral student of the Programa de Doctorado en Ciencias Biomédicas at Universidad Nacional Autónoma de México (UNAM) and has received a fellowship (No. 779947) from Secretaría de Ciencias, Humanidades, Tecnología e Innovación (SECIHTI, formerly CONAHCYT). K.M. is a student in the Biomedical Sciences Doctorate Program of UNAM (519010253) and received a fellowship from SECIHTI (860967). A.M.M. is a student in the Biological Sciences Doctorate Program of UNAM with student number 520009954 and received a fellowship from SECIHTI (1003288). This paper serves as a fulfillment of A.M.M. for obtaining a Ph.D. degree in the Biological Sciences Doctorate Program, UNAM.

Author contributions

M.S., A.M.M, K.M. and V.d.L. trained the monkeys and recorded the data. V.d.L. wrote the initial draft of the manuscript. M.S., A.M.M. and V.d.L. analyzed the data. All authors contributed to the scientific content of the work.

Correspondence and requests for materials should be addressed to V.d.L. (lafuente@unam.mx)

Declaration of interests

The authors declare no competing interests.